Hyperspectral Satellite Radiance Atmospheric Profile Information Content and Its Dependence on Spectrometer Technology

William L. Smith, Henry Revercomb, Elisabeth Weisz, David Tobin, Robert Knuteson, Joseph Taylor, and W. Paul Menzel

***Abstract*—Satellite vertical atmospheric sounding was initiated more than 50 years ago and has evolved to provide the most critical component of today's global observation system. However, the operational use of today's polar orbiting satellite hyperspectral infrared (IR) observations in numerical weather prediction (NWP) has been limited to a small fraction of the radiance information being provided. On the other hand, research systems are in operation that combines high vertical resolution polar hyperspectral radiance measurements with high spatial and time resolution geostationary multispectral radiance measurements that demonstrate the promise of future geo-hyperspectral sounding observations to significantly improve the forecast location and warning time for the development of localized tornadic storms. This article has a twofold objective: 1) to demonstrate that there is much more information available in current IR sounding data, than is being used to benefit the current NWP operation and 2) to illustrate the importance of the spectrometer technology (i.e., Fourier transform vs. dispersive grating) used for achieving the vertical profile resolution required to improve both extended range and localized severe weather forecasts. These objectives are achieved by performing both theoretical physics-based radiance information content (IC) studies and empirical analyses of current hyperspectral radiance measurements. The IC studies clearly demonstrate the unique importance of longwave IR (9−15 μm) radiance observations. The empirical studies demonstrate the importance of using Fourier transform spectrometers for providing the high spectral fidelity needed to resolve the small-scale vertical features in atmospheric temperature and moisture profiles, which impact weather forecast accuracy.**

***Index Terms*—Information content (IC), infrared (IR) hyperspectral sensors, satellite remote sensing, weather prediction.**

I. Introduction

THE hyperspectral satellite sounding radiances are routinely assimilated in operational global and regional numerical weather prediction (NWP) models [1]−[4]. Recently, atmospheric sounding retrievals from these radiances have been successfully assimilated by regional weather research and forecasting models using the same physics and numerical algorithms as the NOAA operational rapid refresh (RAP) and the high-resolution rapid refresh models [5]. The retrievals are assimilated using forecast model background profiles to remove the vertical alias of regression retrievals [6]−[8] so that the dealiased regression retrievals are in theory equivalent to optimal estimation (OE) retrievals [9].

Since hyperspectral sounding instruments contain thousands of spectral channels of information, it is computationally challenging to assimilate all of the spectral radiance measurements at all observation locations. However, because the number of model levels is more than an order of magnitude smaller than the number of spectral radiance channels, assimilating all of the spectral information content (IC) through profile retrieval greatly increases the computational efficiency of the assimilation process and enables the use of all the measurements. As explained in Section IV-A, the retrieval is stabilized by compressing the radiance spectrum into its first 30 empirical orthogonal function (EOF) amplitudes or principal component scores (PCSs), which are used as predictors for the profile retrieval process [6], [10]. The practical difference between radiance and retrieval assimilation relates to the computational efficiency of handling the physical variables (e.g., clouds, surface skin temperature and emissivity, trace gases, etc.), which must be accounted for when relating the spectral radiances to the forecast model atmospheric temperature and moisture profile variables. In the case of assimilating atmospheric retrievals, the physical variables affecting the interpretation of radiance measurements in terms of atmospheric profiles are handled prior to the data assimilation process using the complete spectrum of radiance measurements [6]. One question to be answered is "How much information is lost in the forecast model data assimilation process by using a small subset of spectral channel radiances rather than using the entire spectrum of radiance measurements?" This question is answered here using the OE information theory of Rodgers [11], which has previously been applied to spectral channel selection for NWP radiance assimilation [12]−[14].

Currently, NOAA is developing a next generation of hyperspectral atmospheric sounding instruments for flight on low earth orbiting (LEO) and geostationary earth orbiting (GEO) satellites. Current satellite sounding instruments, e.g., the

Manuscript received December 21, 2020; revised March 3, 2021 and April 1, 2021; accepted April 3, 2021. Date of publication April 16, 2021; date of current version May 24, 2021. This work was supported by the University of Wisconsin Space Science and Engineering Center under Program SSEC-2022 Program. *(Corresponding author: William L. Smith, Sr.)*

The authors are with the Space Science and Engineering Center, University of Wisconsin-Madison, Madison, WI 53706 USA (e-mail: bill.l.smithsr@gmail.com; hank.revercomb@ssec.wisc.edu; elisabeth.weisz@ssec.wisc.edu; dave.tobin@ssec.wisc.edu; robert.knuteson@ssec.wisc.edu; joe.taylor@ssec.wisc.edu; paul.menzel@ssec.wisc.edu).

Digital Object Identifier 10.1109/JSTARS.2021.3073482

Infrared Atmospheric Sounding Interferometer (IASI) and the Cross-track Infrared Sounder (CrIS), provide radiance measurements within different portions of three different spectral bands: longwave (LW) 665–1250 cm^{-1} (8–15 μm), midwave (MW) 1250–2000 cm^{-1} (5–8 μm), and shortwave (SW) 2000–2500 cm^{-1} (4–5 μm). The LW-band includes the 15 μm carbon dioxide (CO_2) and the 9.6 μm ozone (O_3) bands used for sensing the temperature and ozone profiles of the atmosphere as well as measurements across the 8–12 μm atmospheric window region of weak water vapor lines used for surface skin temperature determination, near surface water vapor retrieval, and cloud properties and dust aerosol concentration sensing. The MW band is the primary water vapor sensing band consisting of water vapor lines with the wide range of absorption strengths needed to profile tropospheric water vapor. The SW band consists of very "clean" water vapor absorption-free wavelengths, enabling attenuation-free measurements of the Earth's surface and cloud properties. The SW and 4.3 μm band of nitrous oxide (N_2O) and CO_2 emission lines are useful for sensing lower tropospheric temperature with high vertical resolution as well as the stratospheric temperature profile. The work [14] discusses, from a historical perspective, the incorporation of all three spectral bands on the satellite instruments developed throughout the evolution of the satellite-sounding program. Potential uses of a hyperspectral sounder in the geostationary orbit are outlined in [15].

The ability to sense fine scale vertical temperature structure with a satellite spectrometer is physically based on being able to resolve the features of the CO_2 emission lines, which are uniformly spaced across the 15 μm band [16]–[18]. This high vertical resolution temperature sounding capability provided the motivation for the hyperspectral infrared (IR) satellite sensors flying aboard current operational satellites [19]. For example, the Joint Polar Satellite System (JPSS) CrIS instrument scans the interferogram to a maximum delay [optical path delay (OPD) 0.8 cm] just long enough to resolve the 1.6 cm^{-1} uniform spacing of the 15 μm band CO_2 lines (i.e., the first CO_2 resonance produced in the LW interferogram centered at +/−0.64 cm due to the uniform CO_2 ~1.56 cm^{-1} line spacing, as shown in Fig. 1). As a result, the spectral radiance emission measurements resolve radiance contributions from in-between individual CO_2 absorption lines, where there is a strong pressure-altitude dependence resulting from the pressure-broadened wings of the CO_2 absorption lines. However, since the size, weight, and power, as well as the instrument design complexity, depends on the wavelength extent of spectral radiance observations to be obtained, a logical question is whether there is a need for the LW-band measurements in future instrument designs. This question is answered by showing the importance of the LW-band from both the theoretical (i.e., spectral radiance temperature and moisture profile IC analysis) and the empirical (LW-band radiance denial retrieval degradation) points of view.

II. Hyperspectral Vertical Resolution Advantage

The hyperspectral resolution sounding concept is based on Shannon information theory, which explains how a small signal, buried in random noise, can be amplified by accumulating repetitive samples, whereby the signal level is amplified more

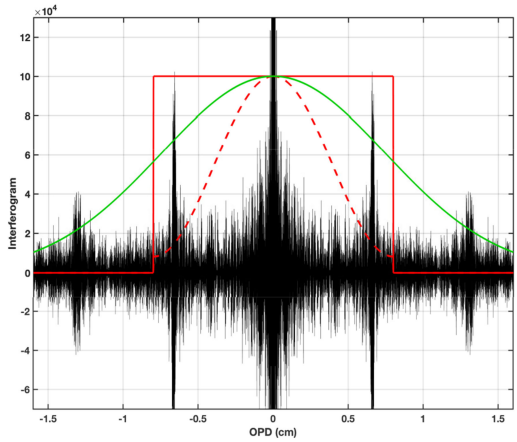

Fig. 1. This interferogram (i.e., the Fourier transform of the spectrum) response functions for the CrIS Fourier transform spectrometer (FTS) and AIRS grating instruments, shown by the solid red box-car and solid green Gaussian-like response functions, respectively. It shows that the FTS for CrIS captures all of the information from the first CO_2 line resonance but none of the second. The AIRS grating is close to CrIS information content because its response to the first and second resonances is combined. The dashed red line shows the Hamming apodization function that is applied to the CrIS data before NOAA uses it for forecast model radiance assimilation.

than the noise level. Claude Shannon, known as "The Father of the Information Age," first explained his theory in 1948 as it related to communication [20]. As an example, Shannon's theory explains how an object can be detected in an image blurred by measurement noise. The object signal may not be detected in a single image because of noise in the signal from surrounding pixels. However, when a time series of multiple images are added together, the object signal amplifies linearly with the number of images while the noise only goes up as the square root of the number. Given a suitable number of images, the viewer can locate the object position within the image frame and identify the object. Exploration for galaxies with the Space Telescope is a great example of this. Hyperspectral sounding behaves in a similar manner when identifying small-scale vertical features buried within the noise level of a set of low vertical resolution radiance measurements. A single measurement cannot "see" fine-scale vertical structure features because a radiance signal arises from a very large depth of the atmosphere as described by the vertical sensitivity function (i.e., the weighting function of the radiative transfer equation) as shown in Fig. 2. However, as one obtains many more spectrally noise independent radiance measurements, small-scale vertical features begin to be resolved as a result of Shannon sampling since the vertical structure signal amplifies more than the surrounding random noise. As more spectral measurements are added, which include the signal from the small-scale vertical feature, the vertical resolution increases enabling the vertical feature of interest to be resolved. This is why hyperspectral sounding instruments have been designed to observe the radiance in thousands of spectral channels.

III. Information Analysis

A. Theory

The theoretical model for defining satellite sounding radiance IC was presented by Rodgers [9], [21]. This model can be

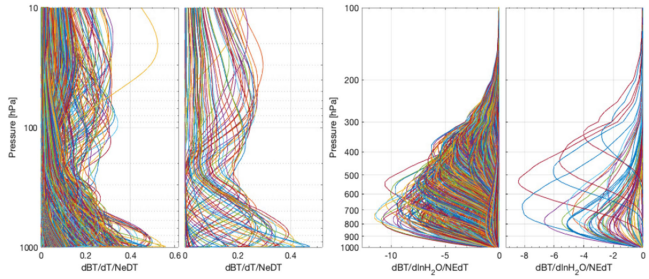

Fig. 2. Brightness temperature (BT) and humidity vertical sensitivity functions, defined as the Jacobians, dBT/dT, and dBT/dlnH$_2$O, divided by the spectral channel instrument noise. The selection of channel sensitivities shown is those that peak at each of the 101 vertical quadrature levels used for the calculation. The left two panels are for temperature sensitivity and the right two panels are for humidity sensitivity. The left panels of the temperature and humidity sets are selected from the full set of CrIS measurement channels, whereas the right panels are for 100 spectral channels that NCEP has used in its assimilation of CrIS radiances within the global forecast system (GFS) model.

used to reconcile the differences between satellite hyperspectral sounding retrievals and radiosondes [22]. It is formulated from OE retrieval theory. In OE, the temperature or water vapor profile is retrieved from radiance measurements through the inverse solution of the radiative transfer equation, conditioned by the use of an *a priori* estimate of the profile and an atmospheric profile covariance matrix describing the statistical uncertainty of the *a priori* condition. The radiative transfer equation is

$$\mathbf{y} \;=\; \mathbf{K}\mathbf{x} + \varepsilon \tag{1}$$

where $\mathbf{y}$ is a vector of spectral channel radiances of dimension m, $\mathbf{x}$ is a vector of the temperature and moisture profile values of dimension n, $\mathbf{K}$ is an $m \times n$ matrix of the vertical weighting functions values for each spectral channel and vertical level of the profile temperature and moisture $\mathbf{x}$, and ε is a vector of measurement errors contributing to the radiance measurement vector $\mathbf{y}$. The OE inverse solution for $\mathbf{x}$, i.e., the retrieval $\hat{\mathbf{x}}$, is given by Rodgers (1990) as

$$\hat{\mathbf{x}} = \mathbf{x}_{ap} \;+ \hat{\mathbf{S}}\mathbf{K}^T\mathbf{S}_{\varepsilon}^{-1}\left(\mathbf{y} - \mathbf{K}\mathbf{x}_{ap}\right) \tag{2}$$

where $\mathbf{x}_{ap}$ is the *a priori* (or background) state estimate and

$$\hat{\mathbf{S}} = \left(\mathbf{K}^T\mathbf{S}_{\varepsilon}^{-1}\mathbf{K} + \mathbf{S}_{ap}^{-1}\right)^{-1} \tag{3}$$

is the estimation (or retrieval) error covariance matrix $\hat{\mathbf{S}}$. This matrix is a measure of retrieval accuracy and depends on $\mathbf{S}_{\varepsilon}$, the measurement error covariance matrix, and $\mathbf{S}_{ap}$, the *a priori* or background covariance matrix.

The sensitivity of the retrieval to the true state, i.e., $\partial\hat{\mathbf{x}}/\partial\mathbf{x}$, is the averaging kernel matrix $\mathbf{A}$ of dimension $n \times n$, which can be written as

$$\mathbf{A} \;= \hat{\mathbf{S}}\,\mathbf{K}^{\mathbf{T}}\mathbf{S}_{\varepsilon}^{-1}\mathbf{K}. \tag{4}$$

The rows of $\mathbf{A}$, which are called averaging kernels or smoothing functions, reflect how the true state is reproduced by the retrieved state, and the width of each averaging kernel can be regarded as a measure of vertical resolution of the observing system.

The averaging kernel matrix $\mathbf{A}$ can be related to both the IC H of a measurement and the degrees of freedom (DoF) for signal d_s; the latter gives the number of independent pieces of information that can be measured. The IC of a measurement, defined as the factor by which knowledge of a quantity is increased by making the measurement, is the reduction of entropy and can be expressed by

$$\begin{aligned} H \;&= \frac{1}{2}\log_2\left|\hat{\mathbf{S}}^{-1}\mathbf{S}_{ap}\right| = \frac{1}{2}\log_2\left|\left(\mathbf{K}^T\mathbf{S}_{\varepsilon}^{-1}\mathbf{K} + \mathbf{S}_{ap}^{-1}\right)\mathbf{S}_{ap}\right| \\ &= -\frac{1}{2}\log_2\left|\mathbf{I}_n - \mathbf{A}\right| \end{aligned} \tag{5}$$

since $\partial\hat{\mathbf{x}}/\partial\,\mathbf{x}_{ap} = \mathbf{I}_n - \mathbf{A}$ is the sensitivity of the retrieval to the *a priori*, and $\mathbf{I}_n$ is the n-dimensional identity matrix. The DoF for signal d_s are given by

$$d_s = \;\mathrm{trace}\left(\mathbf{A}\right). \tag{6}$$

The diagonal of $\mathbf{A}$ can therefore be viewed as a measure of the DoF per level, whereas the reciprocal value as the number of levels per degree of freedom [9].

It can be seen that the IC H and the DoF d_s are closely related to each other since both describe the change in the knowledge of the atmospheric state consequent on taking a measurement, and both measures are characterized with respect to the *a priori* [23].

To compute the retrieval error (i.e., the square roots of the diagonal elements of $\hat{\mathbf{S}}$), the IC H and DoF d_s are computed according to (4)–(6) for a set of noisy measurements. The appropriate estimates of the temperature and humidity *a priori* error as well as of the measurement error are assumed, as described below, to construct the $\mathbf{S}_{ap}$ and $\mathbf{S}_{\varepsilon}$ matrices, respectively. For example, $\mathbf{S}_{ap}$ can be taken as the covariance of the differences between an analysis of profile measurements (e.g., radiosonde observations) and the 12-h forecast of these atmospheric profiles. In the following sections, terms $\hat{\mathbf{S}}$, H, and d_s are computed for several different measurement configurations in order to answer the question regarding the need for an LW spectral band in future instruments.

B. Implementation of Optimal Estimation Theory

Rodgers's information theory, as summarized in Section III-A, applies to radiance IC of atmospheric profiles if they are known *a priori*, rather than to be measured. Therefore, to use Rodgers's OE information theory to define spectral band requirements for a future satellite sounding instrument, two important implementation procedures, not described by Rodgers, are necessary because the atmospheric temperature and moisture profiles cannot be assumed to be known prior to their measurement. The two important implementation procedures that need to be applied when using the Rodgers's OE equations are as follows. 1) A dry atmospheric condition must be assumed to compute temperature profile IC in order to exclude water vapor radiance contributions. Water vapor is a highly variable emitting gas whose profile cannot be assumed to be known prior to its measurement. Failure to exclude water vapor radiance contributions will result in an excessive MW band contribution

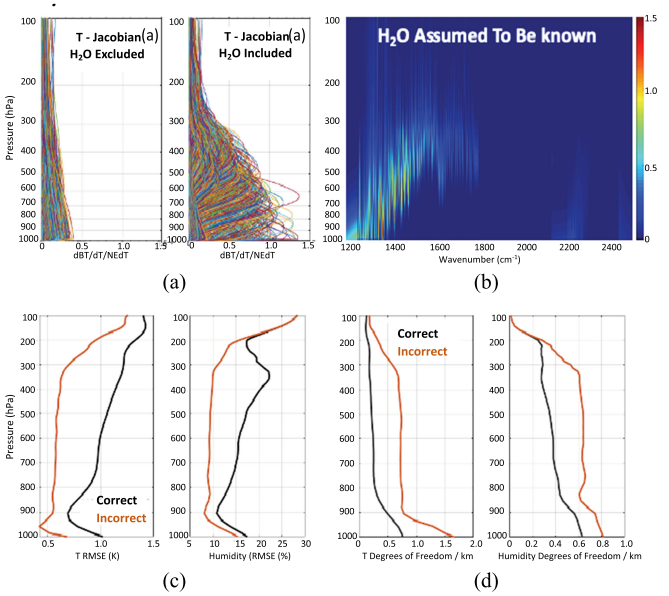

Fig. 3. (a) Atmospheric temperature profile weighting functions, divided by spectral channel noise, (b) spectrum of weighting functions, divided by noise, (c) retrieval accuracies, and (d) degrees of freedom for midwave plus shortwave spectrometer estimated by "incorrect" inclusion and "correct" exclusion unknown water radiances contributions to the temperature profile weighting functions used in the OE estimation process. The water vapor results for the "correct" case also show the effect of temperature error contribution to the water vapor profile accuracy and information content (i.e., degrees of freedom).

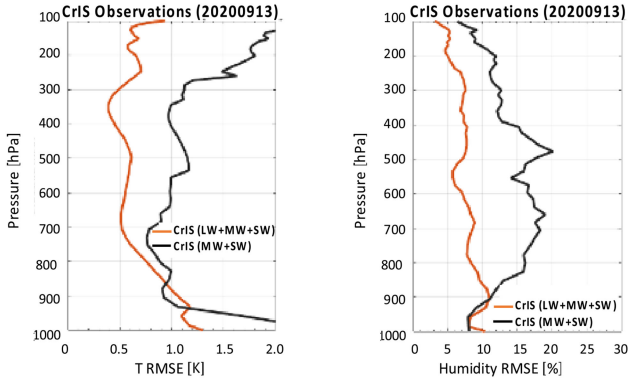

Fig. 4. Real CrIS retrieval accuracy using LW+MW+SW bands vs. only the CrIS MW+SW bands. These results validate the "correct LW+SW" theoretical expectations shown in Fig. 3.

to the temperature profile IC and retrieval accuracy estimates. 2) For the calculation of the moisture profile IC and profile retrieval accuracy, the water vapor density error dependence on temperature retrieval error must be included. For a given atmospheric pressure, the water vapor density dependence on atmospheric temperature (i.e., dQ/dT) is described by the ideal gas law for moist air. Therefore, the total water vapor profile retrieval accuracy, which is used to define the water vapor profile IC, needs to be defined as the sum of the radiance determined mixing ratio profile retrieval error and the mixing ratio profile error resulting from the water vapor density error associated with the temperature profile retrieval error. This is accomplished by first computing the OE estimates of radiance-related temperature and water vapor profile error covariances. Then an additional water vapor error covariance is computed from the temperature profile error covariances using the ideal gas law for moist air. The total water vapor error covariances are then estimated as the sum of the radiance and temperature profile error-related water vapor error covariances.

Fig. 3 illustrates the severe misrepresentation that results in temperature profile weighting functions and temperature and water vapor profile retrieval accuracy and IC for a MW plus SW band instrument, if the two implementation procedures to the OE theory, described above, are not made. The top row of panels shows the temperature Jacobians (i.e., weighting functions) divided by spectral channel noise, for the combined CrIS instrument MW and SW bands. These weighting functions are computed by a radiative transfer model with the US Standard Atmosphere 1976 profile as the input. The upper left-hand panel of Fig. 3(a) shows the Jacobians when water vapor contributions are correctly excluded, whereas the right-side panel of (a) shows the incorrect Jacobians that result if the water vapor radiance contributions are included in the computation of the temperature Jacobians. As can be seen from the panel (b) display of the Jacobian spectrum, the very sharply peaked Jacobians shown in the right side of panel (a) are provided by the CrIS MW water vapor spectral channel radiances. The sharpness of the temperature profile Jacobians is due to the exponential decay of water vapor mixing ratio with altitude. However, for the purpose of specifying the spectral radiance measurement requirements for a new sounding instrument, the water vapor radiance contributions to the temperature profile IC and retrieval accuracy estimates must be excluded from OE estimations since the concentration profile for highly variable water vapor is unknown prior to its measurement. Thus, only radiance contributions by the uniformly mixed atmospheric gases, such as CO_2 and N_2O, whose concentrations are well known, should be used for estimating spectral radiance temperature profile IC and retrieval accuracy.

The bottom four panels show the comparison between the retrieval accuracy (RMSE) and DoF per 1-km layers that result when the water vapor radiance contributions are included ("incorrect") and excluded ("correct") from the OE theoretical temperature profile information and retrieval accuracy determination. As can be seen, the inclusion of water vapor radiance leads to a misguided conclusion that a high degree of IC and retrieval accuracy can be achieved with a MW+SW band spectrometer system.

The incorrect theoretical estimation of the capability of a MW+SW instrument is confirmed by comparing actual CrIS radiance profile DRDA retrievals (see Section IV-A) for September 13, 2020 with NWP model forecasts using radiosonde measurements. In Fig. 4, profile retrieval differences with the radiosonde-based model profiles obtained using all three CrIS measurement bands (i.e., LW+MW+SW) with those obtained using only CrIS MW+SW radiance measurements. It can be seen that there is a large increase in the retrieval errors when only the MW+SW bands are used. This increased error is similar

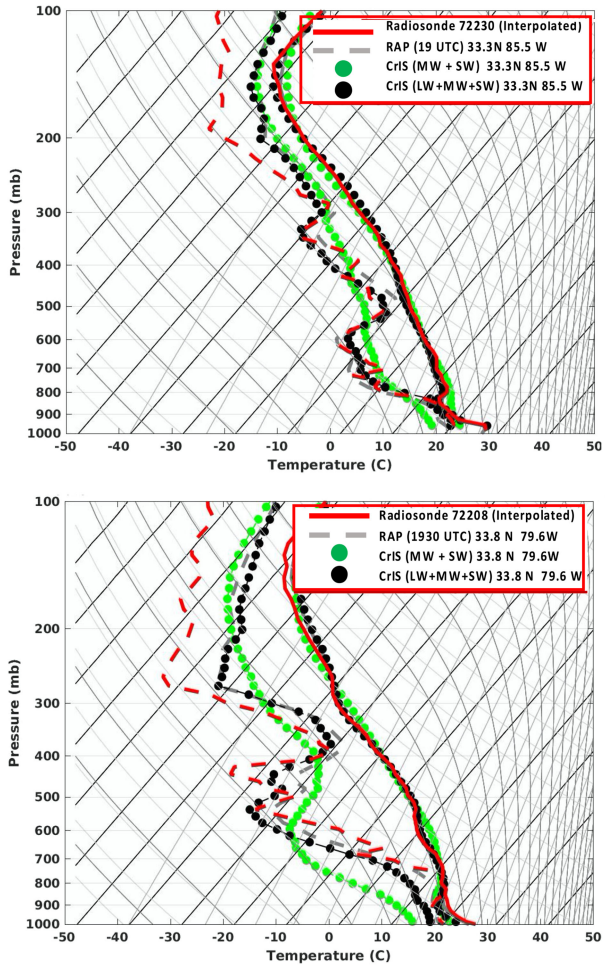

Fig. 5. Skew-T diagrams for September 13, 2020 showing comparisons between radiosonde temperature and dewpoint observations (red lines) with CrIS temperature and dewpoint profile retrievals obtained "with" (black dots) and "without" (green dots) LW-band radiance measurements. The radiosonde profiles shown were space and time interpolated to the CrIS measurement locations and observation times. The NOAA 2-h rapid refresh (RAP) forecast temperature and dewpoint profiles are shown by the gray solid and dashed lines, respectively.

to the increase in the theoretical estimation of retrieval error, shown in Fig. 3, that occurs when unknown water vapor radiance contributions are correctly excluded (i.e., the "correct" results) from the profile theoretical IC and retrieval error OE process. The CrIS temperature and humidity profile errors are reduced dramatically by including the LW-band in the profile retrieval process.

Finally, the implied importance of the LW-band for temperature and water vapor retrieval shown above is more clearly illustrated using a couple of example radiosonde comparisons shown in Fig. 5. The retrievals are obtained using the algorithm described later in Section IV-A. It is very easily seen that the vertical resolution and associated absolute accuracy is degraded greatly when the LW radiance band is excluded from the temperature and water vapor retrieval process. This degradation in vertical resolution is most striking for the near-surface planetary boundary layer (PBL) for both temperature and water vapor

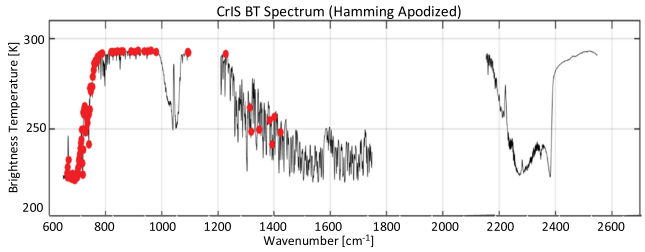

Fig. 6. The 100 spectral channel positions (red dots) of the CrIS channels that NCEP uses for the assimilation of radiances within its global forecast system (GFS) model.

dewpoint as well as for dewpoint temperature throughout the entire troposphere. These examples are consistent with the error statistics obtained from three days of radiosonde comparisons to be described in Section IV-B.

In conclusion, the results show that when the Rodgers's OE information theory is applied properly for specifying the spectral requirements for a new satellite sounding instrument, the sounding capabilities of a MW+SW band instrument are greatly inferior to satellite instruments that include the LW-band. This theoretical result is shown to be consistent with current satellite observations. It is shown that failure to apply Rodgers's IC theory properly, for the purpose of specifying a future IR sounding instrument's measurement requirement, can lead to the misguided belief that the traditional LW-band is no longer needed for NWP applications of satellite sounding radiance data.

C. Dependence on Spectral Resolution and Number of Spectral Channels

As an example, the CrIS instrument spectral channel and noise characteristics were used to assess the difference between the Shannon information content [IC or H from (5)] and DoF [DoF or ds from (6)] for a 100 spectral channel set of observations that NCEP has used for radiance assimilation and for that obtained using the entire spectrum of spectral channels observed by the CrIS instrument. Fig. 6 shows the spectral positions of the 100 CrIS radiance channels that NCEP has assimilated into its global forecast system (GFS) model, along with the spectral range of the LW, MW, and SW measurements. As can be seen, only channels within the LW and MW of CrIS are assimilated.

The NCEP assimilated CrIS radiance spectra are Hamming apodized. This apodization suppresses the negative side lobes of the unapodized sinc line shape, but also introduces significant spectral correlation of both the signal and noise among neighboring spectral channels. This correlation can be removed exactly, and the original full spectral resolution (FSR) and IC retained, if the correlation due to Hamming apodization is specified in the assimilation process and all neighboring spectral channels are utilized. However, the NCEP channel set does not include neighboring spectral channels. For example, in the LW temperature sounding region, every other spectral channel is selected between 678.75 and 710 cm^{-1} and between 713.75 and 747.5 cm^{-1}.

TABLE I
CRIS TEMPERATURE AND HUMIDITY PROFILE RADIANCE INFORMATION CONTENT AND DEGREES OF FREEDOM FOR FULL CRIS AND NCEP 100 CHANNEL SETS

	Full CrIS		NCEP CrIS	
	Temperature	Humidity	Temperature	Humidity
Information Content	34.4	32.0	26.8	17.6
Degrees of Freedom	10.1	6.5	7.6	3.4

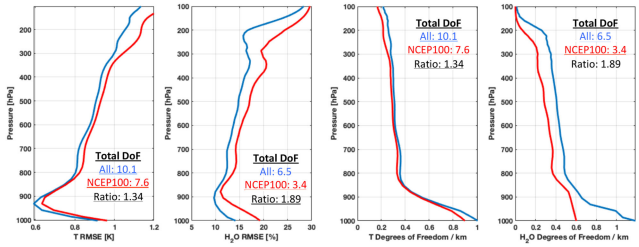

Fig. 7. Optimal estimation radiance assimilation model profile RMS error, and vertical degrees of freedom (DoF) for the CrIS NCEP 100 spectral channel set (red) and all spectral channel (blue) cases. These results are based on forecast model background error covariance matrices for a 2 K and 30% RMSE for temperature and humidity, respectively. The vertical error correlation length was assumed to be 3 km.

Table I shows the IC and DoF values for the NCEP 100 channel radiance assimilation system and that for the full CrIS spectral channel measurement system. For these calculations, the in-orbit NOAA-20 measured detector average CrIS spectral noise are used together with a background error covariance matrix (S_{ap}), simulated to be representative of typical current model forecast errors. For the simulated forecast model error covariance matrix definition, root mean square (rms) forecast errors of 2 K and 30% are assumed for temperature and humidity, respectively, with an error vertical correlation length of 3 km. Hamming apodization was applied to the spectral weighting functions for the NCEP 100 channel case, while the CrIS weighting functions were left unapodized for the full CrIS channel case. For the NCEP 100 channel case, the CrIS noise is reduced by the Hamming apodization factor of 0.65. As can be seen from Table I, for atmospheric temperature, there is a 34%, or greater, difference between full CrIS and NCEP CrIS DoF. For humidity, the differences are even larger being nearly a factor of 2 (i.e., 1.89).

The vertical distribution of model profile rms error and vertical resolution for the "NCEP 100 channel CrIS" and "All-Channel full CrIS" observation cases after radiance assimilation are shown in Fig. 7. The differences are much greater for atmospheric water vapor than they are for atmospheric temperature as would be expected from the much larger number of temperature sounding channels than water vapor sounding channels used by NCEP, as was shown in Fig. 6.

Although the difference in the rms errors for the two spectral channel data sets appear to be small, they are actually quite significant considering that these are 1-sigma rms errors, meaning that these values represent the expectation of the smallest 66% of the profile retrieval errors. In reality, 2 sigma or greater Gaussian distribution retrieval errors might be expected for the more complex vertical structures associated with storm development atmospheric conditions. It can be seen that by multiplying the 1-sigma errors by factors of 2, or more, the retrieval errors could easily exceed the model background accuracies of 2 K and 30%, making the satellite radiances useless for reducing the model background error necessary for improving numerical forecasts. It is also important to note the differences in atmospheric profile accuracy and vertical resolution for these two channel data sets for the temperature and humidity within the near surface PBL. These differences are significant because the accuracy of the initial condition in the numerical model PBL is crucial for forecasting convective storms. Probably the best measure of the IC difference between the NCEP 100 channel radiances and the full CrIS radiance spectrum is expressed by their differences in total DoF, computed via (6). It can be seen that using a small set of spectral channels, even if carefully chosen as it was for the NCEP channel set, results in a large loss of the information contained in all of the CrIS spectral channels.

Opposed to the use of nonadjacent channel sets, other assimilation centers have utilized full covariance matrices and channel sets with neighboring channels to retain more of the full CrIS IC. The work [24], for example, describes this approach where many neighboring channels from 686.875 to 739.375 cm^{-1} are utilized, and a significant improvement in forecast impact is realized.

D. Information Content of the LW-Band

As discussed in Section III-B, an important question is whether or not a requirement for an LW-band is needed for future LEO and GEO atmospheric sounding instruments. The LWIR observations are critical to weather forecasting for the following reasons.

1) The LW-band provides the highest vertical resolution temperature sounding measurements in the middle and upper troposphere and lower stratosphere, including the tropopause height, by resolving the 15-μm CO_2 band absorption line spacing.
2) The LW-band provides radiance measurements that are not contaminated by reflected sunlight, which otherwise restricts the utility of the SW band for lower tropospheric temperature profiling.
3) The LW-band provides spectral radiance measurements across the 9−12 μm "window" region used for surface skin temperature measurements, cloud top ice/water phase, important for forecasting aircraft icing, near surface (PBL) water vapor profile measurements over land and sea, and the detection of dust aerosol concentration and layer top altitude.
4) The LW-band provides observations of atmospheric ozone through its 9.6-μm O_3 band radiance spectrum measurement capability.

It is also important to note that the SW-band has an advantage relative to the LW-band of observing near surface temperature profiles and surface skin temperature due to low water vapor absorption but only if there is no sunlight contribution to the

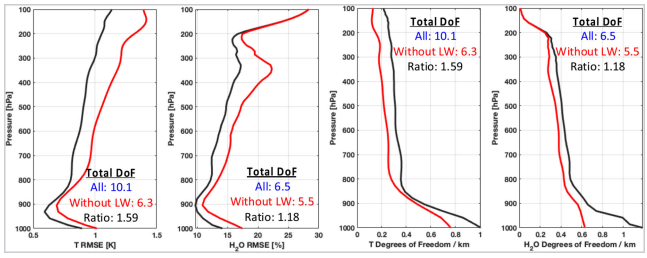

Fig. 8. Model profile rms error and vertical degrees of freedom for an "All" channel CrIS instrument (black line) with an instrument that excludes the LW-band channels (red line).

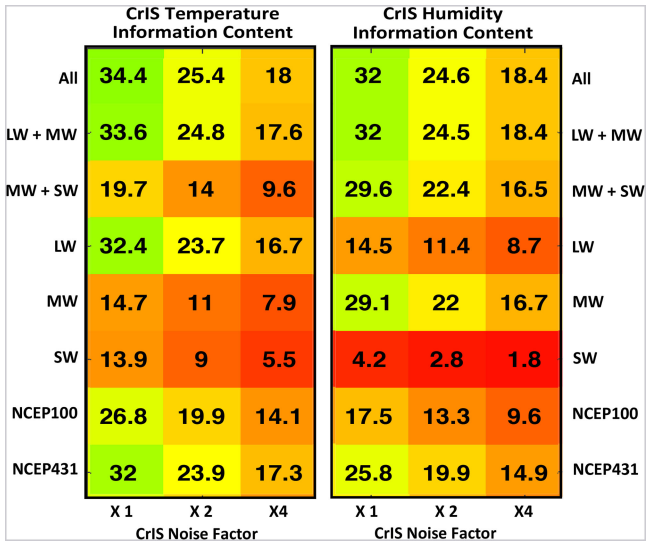

Fig. 9. CrIS spectral radiance information content for various assumed spectral channel combinations and noise levels associated with optimal estimation profile retrieval or NWP model radiance assimilation.

observed radiances. For the upper atmospheric temperature, the interpretation of the SW-band radiance measurements is complicated by emission departures from Planck's law due to nonlocal thermodynamic equilibrium. In order to determine the LW-band temperature and moisture sounding IC, the Rodgers's OE analysis method discussed in Section III-A was applied in accordance with the implementation approach described in Section III-B assuming CrIS FSR measurement characteristics and NOAA-20 instrument in-flight noise levels. As was assumed in Section III-C, for defining the radiance measurement impact on forecast model OE profile specifications, typical model background temperature, and humidity errors of 2 K and 30%, respectively, were assumed with a profile error covariance vertical correlation length of 3 km.

The CrIS spectral measurement characteristics are assumed for each of its three spectral bands (i.e., LW, MW, and SW). Fig. 8 shows the results of the vertical distribution of model profile rms error, the DoF profiles, as well as the total atmospheric column DoF, after radiance assimilation. The assimilation of the full three-band CrIS instrument channel radiance set is compared to the results obtained with the CrIS instrument if the LW-band is excluded. Similar to the empirical measurement results shown earlier in Fig. 4, Fig. 8 shows that a large loss of temperature profile information (a total of about 60%) occurs when the LW-band is excluded. Most important, it shows that there is a large degradation in the vertical DoF (i.e., the inverse of the vertical resolution) of both the temperature and the water vapor profile in the near surface PBL, which is most important for convective storm prediction. The reason why the LW-band has a large influence on near surface water vapor is because the 8−12 μm "window" spectral region contains a large number of weak water vapor lines, which together with the contribution of the water vapor continuum, makes the LW-band "window" measurements highly sensitive to near surface water [27].

E. CrIS Instrument Radiance Information Content

Fig. 9 illustrates CrIS spectral radiance IC for various assumed spectral channel combinations assumed for OE profile retrieval or NWP model radiance assimilation. The cases highlighted in green denote those spectral band combinations and noise levels that provide a large amount of the CrIS radiance IC, while those highlighted in yellow and yellowish green provide a moderate amount of CrIS IC. The orange to red highlighted cases denote a small amount of the CrIS IC provided for NWP data assimilation purposes. Although the absolute values shown in Fig. 9 assume a perfect radiance calibration and forward radiative transfer model, they do represent the relative IC of various band combinations.

IV. Analysis of Simultaneous AIRS and CrIS Radiances and Retrievals

The evolution of hyperspectral IR remote sounding systems useful for obtaining high vertical resolution sounding observations began during the mid-1980s with the first successful flights of the University of Wisconsin (UW) high-resolution interferometer sounder (HIS) [17]−[19] on the high-altitude NASA ER-2 aircraft. This was followed by space flights of the NASA Advanced Infrared Sounder (AIRS) in 2002 on the Aqua satellite [28], the European IASI beginning in 2007 [29] on the Metop series of satellites, and the NOAA CrIS in 2011 [30] on the SNPP satellite followed by the JPSS CrIS instrument on the NOAA-20 spacecraft in 2017.

Because the Aqua, the SNPP, and the NOAA-20 satellites are in the same orbit but at different altitudes, the AIRS and the CrIS instruments view North America at almost the same time every 2.5 days. Comparisons have been made between AIRS and CrIS retrievals, derived with the dual regression plus de-aliasing (DRDA) method [7], and radiosondes and RAP model soundings over the North American region (24–45 N, 70–100 W) for three days in August and September 2020.

A. DRDA Retrieval Methodology

The atmospheric profile retrieval algorithm used for the comparison of AIRS and CrIS retrievals is the physically based dual regression (DR) algorithm [6] combined with a physical

vertical resolution de-aliasing (DA) step to enhance the vertical resolution of the regression retrieval [7]. DR is a single field-of-view (FOV), all-sky condition, retrieval algorithm developed to provide atmospheric soundings along with surface and cloud parameters simultaneously from any of the operational hyperspectral sounders orbiting the Earth. DA is a fast-physical tool to enhance the vertical resolution of the DR result using a forecast model background forecast as a constraint on the final DRDA retrieval [7], [8]. The DA step uses the difference between the observed radiance spectrum and that associated with the forecast model background profile, computed using the principal component radiative transfer model (PCRTM) [31], [32], a fast-forward spectrum-based radiative transfer model. Simply explained, the calculated satellite radiance spectrum is that spectrum that would have been observed if the true atmospheric profile was the same as the model background profile. The simulated radiance spectrum is then used to perform a DR retrieval using the exact same regression relations used to obtain the original (observed radiance) DR retrieval. The vertical alias of the regression retrieved profile is the difference between the simulated radiance DR retrieval and the model background profile, which can then be removed from the observed radiance DR retrieval. The vertical DA process is particularly important for NWP model assimilation of the profile retrieval data since the profile retrievals have a vertical resolution consistent with the vertical resolution of the model background field into which the retrievals are being assimilated. DRDA has an important computational efficiency advantage over the use of OE in the assimilation process since there is no need for the DRDA retrieval solution to be iterated to account for Jacobian errors resulting from errors in the model background profiles used as the *a priori*. DRDA only requires a single radiative transfer calculation using the model background since the Jacobian is accounted for within the regression solution used for the DA process. The retrieval is stabilized by compressing the radiance spectrum into its first 30 EOF amplitudes (i.e., PC scores), which are used as predictors for the profile regression retrieval [10]. For clear skies, this process makes the IC from retrieval assimilation equivalent to that of radiance assimilation, as long as the same spectral resolution, number of spectral channels, and instrument and forward model noise levels are used for the data assimilation process [33].

The DRDA retrieval approach produces accurate high vertical resolution retrievals useful for NWP data assimilation [5]. In order to illustrate the high vertical resolution characteristics of the DRDA retrievals, Figs. 10 and 11 show results from comparisons of CrIS retrievals with radiosonde balloon measurements. Also shown are results for colocated retrievals produced near the radiosonde observations using the NOAA/NESDIS operational NUCAPS retrieval algorithm [34]. The NUCAPS all-sky retrievals, which are obtained from the combination of IR and microwave radiances measurements, are a Level-2 product of the CSPP software [35] used to process direct broadcast satellite data. NUCAPS and DRDA are similar in that both algorithms use EOF regression [10], commonly called principal component (PC) regression, to initialize a physical retrieval based on the difference between observed and initial profile calculated

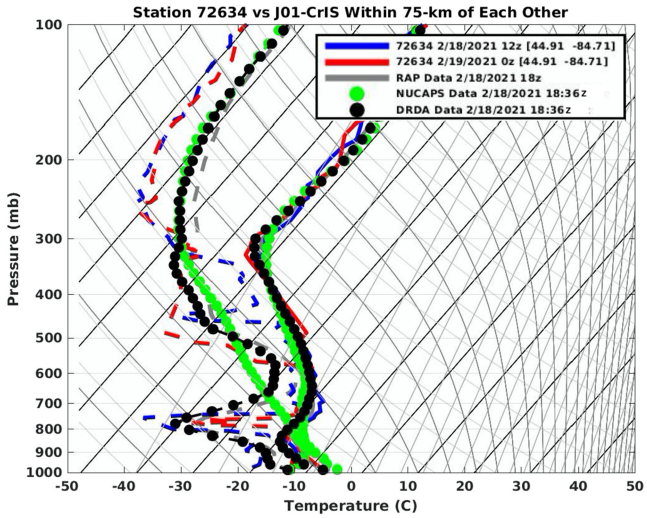

Fig. 10. Colocated DRDA and NUCAPS atmospheric profiles retrieved from CrIS radiance measurements at 18:36 UTC compared with radiosonde measurements made from the NWS upper air station 72634 (Gaylord MI) on February 18, 2021 (12 UTC shown in blue) and February 19, 2021 (00 UTC shown in red). The solid curves are for temperature and the dashed curves are for dewpoint. The black curves denote the DRDA CrIS retrieval, whereas the green curves denote the NESDIS operational NUCAPS combined CrIS/ATMS retrievals, and the gray curves represent the RAP 2-h forecast at the satellite CrIS location at 18 UTC).

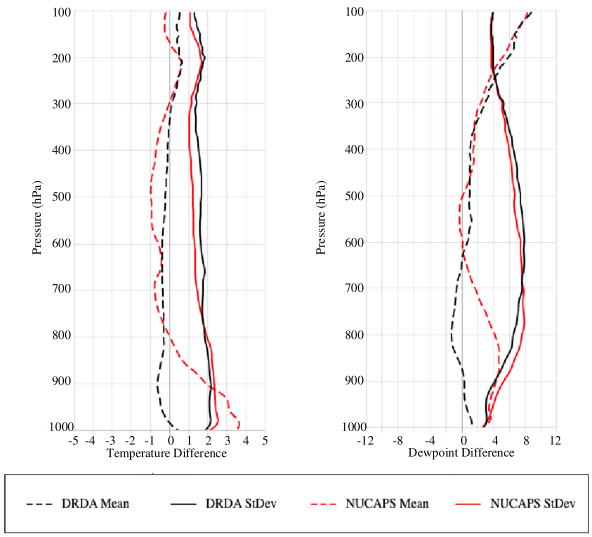

Fig. 11. Accumulative mean and standard deviation of differences (in degrees Kelvin) between space and time colocated DRDA and NUCAPS retrievals and CONUS radiosondes for the period November 25, 2020 to February 25, 2021. The 00 UTC and 12 UTC radiosondes were time interpolated to the CrIS satellite observation times for these comparisons obtained from HU website [35].

radiances. The main difference between NUCAPS and DRDA is that NUCAPS is a 50-km horizontal resolution all-sky cloud condition IR plus microwave retrieval, whereas DRDA is an IR instrument single FOV ($\sim$15 km) retrieval for the clear atmosphere above clouds and between a broken cloud cover. Both NUCAPS and DRDA use NWP model data to initialize their physical retrieval steps; NUCAPS uses eigenvector regression retrievals trained on ECMWF model analyses and CrIS

cloud-cleared radiances while DRDA uses RAP 2-h forecast profiles for its vertical DA step of the physical retrieval process. For the results shown in Figs. 10 and 11, both the DRDA and the NUCAPS retrievals have been averaged within a 75-km radius of the radiosonde station locations in order to minimize differences due to the different horizontal resolution of the two retrieval products.

The profile comparison shown in Fig. 10 was selected to show characteristics typical of the daily retrieval/radiosonde comparisons, which can be viewed on a daily basis at the Hampton University (HU) website, accessed using [36]. The general conclusion that can be drawn from these comparisons, as shown in the Fig. 10 example, is that the vertical resolution of DRDA retrievals is higher than that produced by the NESDIS NUCAPS algorithm. This is particularly true for moisture (i.e., dewpoint temperature) and within PBL (i.e., surface to 700-hPa level). The high vertical resolution advantage of DRDA is a consequence of using the operational RAP model forecast profiles (the gray colored profiles in Fig. 10) as a constraint within the DA step of the DRDA retrieval process. It is also important to note that the DRDA retrievals are generally in better agreement with the radiosonde observations than are the RAP model forecast profiles used to vertically de-alias the satellite DR retrievals. Fig. 11 shows an example of statistics (i.e., mean and standard deviation) between colocated DRDA and NUCAPS CrIS retrievals and two months of time interpolated 00 UTC and 12 UTC radiosonde observations from upper air stations within 75 km of the CrIS radiance observations [36]. One can see that the DRDA retrievals in the lower troposphere (600- to 1000-hPa) are in closer agreement with the radiosonde observations than are the NUCAPS retrieved profiles, believed to be due to the DRDA retrieval vertical DA within the vertically structured PBL. The fact that the NUCAPS standard deviation for temperature and humidity above the 600-hPa level is smaller than the DRDA standard deviation is also believed to be due to the difference between NUCAPS and DRDA vertical resolution. The higher vertical resolution DRDA CrIS retrievals are more likely to experience differences due to space and time misregistration with the radiosonde observations, than the vertically smoother NUCAPS retrievals. Also, the insensitivity of the ATMS microwave measurements to thin and/or partial high altitude Cirrus cloud contamination, which impacts the IR CrIS measurements, may also contribute to the lower NUCAPS standard deviation from radiosonde observations at the higher altitudes shown in Fig. 11.

B. Comparison Between AIRS and CrIS Retrievals

AIRS and CrIS radiances and retrievals were collocated spatially so that their geographical spacing was less than 0.1 degree in both latitude and longitude (i.e., $<$11.1 km), which is within the $\sim$15 km, depending on scan angle and FOV size of the AIRS and CrIS instruments. Only pairs determined to be cloud-free for both of the colocated AIRS and CrIS FOVs were used in the analyses. The inclusion of cloudy scene radiances and retrievals would accentuate the differences shown here for relatively uniform clear sky atmospheric scene conditions.

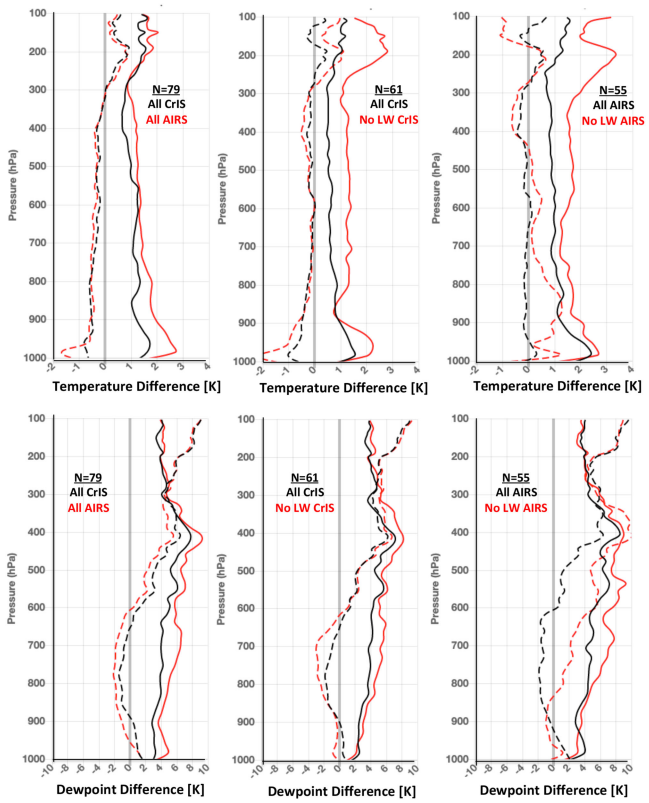

Fig. 12. Comparisons between CrIS and AIRS DRDA retrieved temperature and dewpoint temperature retrieval minus radiosonde profile observations for August 17, 2020 and September 10, 2020. The left-hand panel shows the results for AIRS (red) and CrIS (black) FOV colocated clear-sky retrievals. The center panels and right-hand panels show comparisons between CrIS and AIRS, respectively, colocated "ALL" spectral band and two spectral band (i.e., "No LW" band) deviations from radiosonde observations. Dashed lines are plotted for the mean differences, while the solid lines refer to the standard deviation of the differences. *N* is the number of radiosondes used for the comparisons shown.

AIRS DR and DRDA retrievals were produced from radiances for nominally low-noise spectral channels as selected by the NASA JPL AIRS project. Also, random errors of AIRS measurements are filtered through the use of eigenvector regression [7], [24] for the DR step of the retrieval process. The noise filtering is extremely effective since only 30 EOFs, or PCs, generated from a global annual sample described in [6], are used to noise-filter the 1251 AIRS good channel radiances and 1971 FSR CrIS channel radiances; this provides a spatial/temporal random noise reduction factor close to the square root of (30/1251) and (30/1971) for AIRS and CrIS, respectively. The same number of EOFs, or PC scores, (30) is used as predictors for the AIRS and CrIS regression retrievals. Thus, the use of EOF regression ensures that the differences between CrIS and AIRS retrievals are not due to spatially/temporally random errors in individual channel radiances but instead due to the spectral IC and measurement spectral fidelity differences between the two different instrument systems.

Fig. 12 shows the CrIS and AIRS DRDA retrieved temperature and dewpoint temperature retrieval minus radiosonde profile observations for August 17, 2020 and August, 20 2020 and September 10, 2020. The radiosonde observations used for

the comparisons were interpolated to the location and time of the satellite observations using the difference between the RAP model profiles at the locations and times of the radiosonde and satellite observations as the dependent variable for the interpolation. That is, the radiosonde observation deviation from the RAP for the 00 UTC and 12 ITC radiosonde observation at the radiosonde station location closest to the satellite observation was used to predict, via linear interpolation, the radiosonde deviation from the RAP at the satellite location and observation time. The pseudo-radiosonde profile to be compared to the satellite retrievals was then taken as the RAP values at the satellite location and time added to the interpolated radiosonde/RAP deviation. The left-hand panel of Fig. 12 shows the results for AIRS (red) and CrIS (black) FOV colocated clear-sky retrievals. The center panels and right-hand panels show comparisons between CrIS and AIRS, respectively, colocated "ALL" spectral band (i.e., LW+MW+SW) and MW+SW band (i.e., "No LW" band) deviations from radiosonde observations. Dashed lines are plotted for the mean differences, while the solid lines refer to the standard deviation of the differences. The variations in the number of retrieval comparisons obtained are due to the decrease in the ability to detect clear sky conditions for the "No LW" band condition. The mean differences between the radiosonde and the CrIS and AIRS retrievals are nearly the same since they are both bias corrected using the area domain average difference between the NOAA operational RAP forecast profiles and the retrievals. The "bias correction" used here is similar to that used by NWP centers prior to the assimilation of the satellite radiance data into the forecast model. The standard deviation of the differences between the FOV colocated clear-sky "ALL CrIS" and "ALL AIRS" and radiosonde observations show that CrIS soundings have a better agreement with radiosonde observations, than does AIRS, for both temperature and humidity (i.e., dewpoint temperature). Hence, CrIS soundings are shown to be more accurate than AIRS soundings.

The reason for this accuracy difference relates to CrIS being a Fourier transform spectrometer (FTS), which utilizes the same single detector for all in-band channel measurements, whereas the AIRS is a dispersive grating spectrometer (GS), which uses a separate detector element for each spectral channel radiance measurement within a given spectral band. This basic difference in spectral radiance sampling impacts the spectral fidelity of the radiance spectra being measured. As to be discussed in Section IV-C, the vertical resolution and accuracy of the radiance specified profiles is highly dependent on the spectral fidelity of the radiance measurements being used. Furthermore, Fig. 12 shows that retrieval errors for both instruments increase significantly when their LW-band radiances are excluded from the retrieval process. In particular, the temperature profile errors increase dramatically with altitude and the middle tropospheric humidity (i.e., dewpoint temperature) errors increase greatly, when the LW spectral radiance measurements of these two instruments are excluded from the retrieval process. This empirical result confirms the theoretical OE IC expectations presented for the CrIS instrument earlier in Fig. 3.

Because the number of radiosonde comparisons shown in Fig. 12 is relatively small, being less than 100 radiosonde

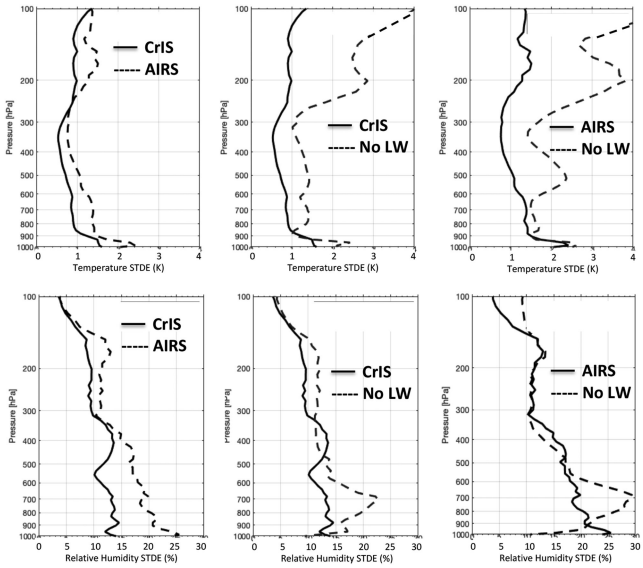

Fig. 13. Temperature and humidity retrieval minus RAP profile differences for August 17, 2020 and September 10, 2020 for 3997 FOV colocated clear-sky retrievals. The left panels show the comparisons between CrIS and AIRS deviations from the RAP profile, the center panels show the differences between CrIS all spectral bands and two spectral bands (i.e., without the LW-band) deviations from the RAP, and the right panels show the differences between AIRS all spectral bands and two spectral bands (i.e., without the LW-band) retrieval deviations from the RAP.

observation comparisons, retrieval error statistics were also determined using NWP model (RAP) analysis profiles as "truth" for radiosonde observation rich areas. In this case, nearly 4000 (i.e., 3997) clear-sky colocated CrIS and AIRS retrievals could be used for their accuracy estimates. Fig. 13 shows the retrieval minus RAP profile difference standard deviations for the August 17, 2020 and September 10, 2020 days used for the radiosonde validations.

The magnitude of the standard deviation of the differences between the retrieved soundings and radiosonde influenced RAP analysis soundings support the conclusions from the smaller number of radiosonde comparisons shown in Fig. 12, that the CrIS soundings have a higher accuracy than the AIRS soundings for both temperature and humidity. Furthermore, as was shown by the radiosonde comparisons, the retrieval errors for both instruments increase significantly when their LW-band radiances are excluded from the retrieval process. Similar to the radiosonde comparison results, these empirical forecast models validated results are in agreement with the theoretical OE IC results presented for the CrIS instrument in Fig. 8.

C. Observed Minus Calculated Radiance Spectral Noise Comparisons

In order to understand the cause for the difference between the AIRS and CrIS retrieval comparisons with RAP, observed minus RAP calculated radiances were compared for each instrument. It is known that the major source of profile retrieval error is the vertical smoothing of the profile caused by the lack of vertical resolution of the radiances used for the retrieval process [20]. The vertical resolution depends on the spectral

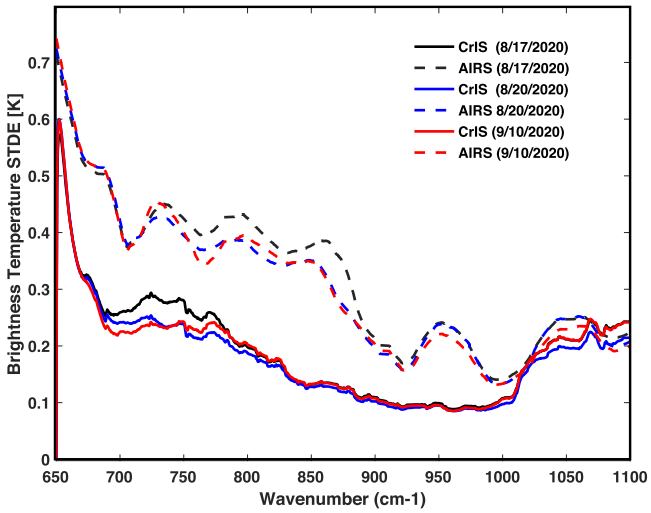

Fig. 14. Smoothed (100-point filtered) standard deviation of "obs-calc" brightness temperature differences for AIRS (dashed) and CrIS (solid) across the LW-band (650−1100 cm^{-1}) of each instrument (650−1100 cm^{-1}).

channel-to-channel radiance artifacts since resolving vertical profile features depend on resolving the signal contained in small differences between spectral channel-to-channel radiance observations within the observed radiance spectrum. As shown below, the AIRS and CrIS retrieval differences found in Figs. 12 and 13 are related to the fact that a single detector is used for all spectral channels within a region (LW, MW, or SW) of an interferometer (FTS) while different detectors are used for each spectral channel within a spectral region of a GS. As a consequence, detector-dependent errors (e.g., detector-dependent calibration error, time variations of spectral responsivity, and detector element coregistration error) can induce spectral channel-to-channel variations for radiance measurements with a GS that does not occur with an FTS instrument, which uses the same single detector for all the spectra radiance measurements obtained within a broad spectral region.

By subtracting a 25 spectral channel ($\sim$15 cm^{-1}) running mean of the difference between the observed AIRS and CrIS spectral channel radiances and the RAP model profile calculated radiances (i.e., "obs-calc") from each individual spectral channel "obs-calc" difference, an estimate of the within-band spectrally dependent "obs-calc" error for each instrument was produced. Averaging over 15 cm^{-1} increments minimizes the influence of spatially and temporally random errors in the measurements, thereby leaving only the spectral channel-to-channel random noise component within the $\sim$15 cm^{-1} increments, which defines the spectral fidelity of the measurement. Fig. 14 shows a 100 spectral point ($\sim$60 cm^{-1}) running average of the spectral channel-to-channel error that can be used to represent the "spectral fidelity" noise for AIRS and CrIS. The AIRS and CrIS spectral fidelity "obs-calc" errors differ by as much as a factor of 2 in the LW-band. It will be shown that this excessive AIRS spectrally dependent error causes the difference in retrieval comparisons shown in Figs. 12 and 13.

In order to make sure that this difference in the AIRS and CrIS estimates of their spectral channel-to-channel random error is not produced by the fact that the CrIS has a slightly different number of spectral channels than the AIRS for the retrieval process, the exact same calculation was performed by using CrIS spectral radiance observations closest to each AIRS spectral channel in place of the actual AIRS radiance observation. The result (not shown here) confirmed that the difference between the AIRS and CrIS spectrally random noise is not due to their slight differences in spectral channels used but, instead, due to their difference in their spectral detector configuration (i.e., the use of a single detector as opposed to the use of multiple detectors) for observing the LW, MW, or SW in-band radiances. Although a newer state-of-the-art grating instrument might improve upon the spectral fidelity associated with the AIRS, the fidelity of the radiance spectrum produced with a multiple detector grating instrument cannot reproduce the degree of fidelity of the spectrum produced using a single detector FTS instrument.

D. Impact on Resolving Profile Vertical Features

The impact in the CrIS FTS vs. AIRS GS radiance spectrum fidelity on vertical resolution of the retrievals is demonstrated with the DRDA retrieval solution, written as

$$\hat{\mathbf{x}} = \mathbf{x}_m + \mathbf{C}\,(\mathbf{y} - \mathbf{y}_m) \tag{7}$$

where $\hat{\mathbf{x}}$ is the retrieved profile vector, $\mathbf{x}_m$ is the forecast model profile vector, $\mathbf{y}$ is the observed radiance spectrum vector, $\mathbf{y}_m$ is the model profile calculated radiance spectrum vector, and the matrix $\mathbf{C}$ is the regression coefficient matrix that relates the spectral radiance differences to model profile variable differences. As can be seen, if the model profile is considered to be "truth," then as the radiance observation approaches the model calculated radiance (i.e., "truth"), the retrieved profile approaches the model, or the "true," atmospheric profile. (Of course, in the general case, the model profile is in error so that the retrieved profile, or model assimilated radiance profile, should be a closer approximation of "true" atmospheric profile than the model profile used as the *a priori* in the retrieval or radiance assimilation process.)

The linear regression retrieval solution can also be described by the OE equation (2) by defining the background profile $\mathbf{x}_m$ as the mean profile of the statistical ensemble of atmospheric profiles used to compute the regression coefficient matrix $\mathbf{C}$, and $\mathbf{y}_m$ is defined as the atmospheric radiance spectrum associated with the statistical ensemble mean profile. In this case, the regression retrieval vertical structure will be biased by the atmospheric structure of the vertically smooth global mean atmospheric profile rather than the more realistic atmospheric vertical structure provided by a dynamical forecast model for the location and observation time of the satellite measurement. That is what motivates the DA step in the DRDA retrieval method [8] to ensure compatibility between the retrieval and the model background prior to the data assimilation process. It is also important to note that the EOF regression [7] is used to suppress the impact of random measurement errors on the retrieval results. In practice, the CrIS and AIRS radiance spectra are transformed to their first 30 pieces of noise-independent spectral radiance information, represented by 30 EOF amplitudes (i.e., PC scores),

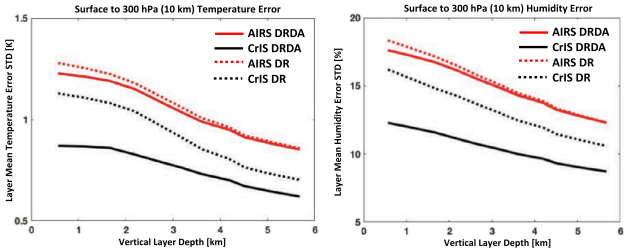

Fig. 15. Relationship between AIRS and CrIS layer mean temperature error with layer thickness within the 0−10 km (surface to 300 hPa) tropospheric region for both the DRDA (solid) and DR (dashed) retrieval methods.

which are then used as the predictors in the initial DR step [6] of the DRDA retrieval process [7].

In order to illustrate the impact of the CrIS and AIRS spectral channel-to-channel random radiance errors on the retrieved atmospheric profile vertical resolution, the tropospheric mean of layer averaged profile retrieval errors was calculated by vertically averaging the retrieval errors used to produce Fig. 13, for different sublayer thicknesses within the surface to 300-hPa (i.e., 10-km altitude) tropospheric layer. If the CrIS and AIRS retrieval error differences are primarily due to the differences in the vertical resolution of their radiance measurements, the tropospheric mean of sublayer vertical mean retrieval errors should decrease with the increase in thickness of the sublayers within troposphere, with the dependence on layer thickness being greater for the CrIS retrievals than for the AIRS retrievals.

Fig. 15 shows the relationship between the vertically averaged AIRS and CrIS sublayer mean temperature and humidity errors within the surface to 10-km level of the troposphere, as a function of the sublayer thicknesses for both the physical DRDA retrieval results and the pure regression DR retrieval results. The DR pure regression results, which are completely independent of the verifying RAP data, essentially show the same characteristics as the DRDA vertical resolution results in that the CrIS tropospheric sublayer errors are much smaller than the AIRS sublayer accuracies for all layer thicknesses. What is most interesting is that, unlike the CrIS retrievals, there is little vertical resolution enhancement of the AIRS regression retrievals by using the RAP forecast profile as an *a priori* estimate of the profile in the DRDA process. In order to understand this result, it is important to note that the main difference between DRDA and regression is the different measurement dimension over which the spectral radiance observation errors are being minimized. In regression retrievals, the observation errors are being minimized over the space/time sample dimension, whereas in DRDA, the observation errors are being minimized over the spectral sample dimension (i.e., the spectral channels within the radiance spectrum). The fact that there is little vertical enhancement of the AIRS retrieval accuracy by increasing layer thickness, relative to the CrIS retrievals, is believed to be a consequence of the GS using a separate detector for each spectral channel radiance observation. That is, for AIRS, there is little difference between the random noise level in the space/time sampling domain and the channel-to-channel noise level in the spectral domain for a single space/time sample of the radiance spectrum. This spectral versus spatial independence of the noise (i.e., the spectral channel-to-channel noise being smaller than the space/time sample detector noise) is absent in the GS radiance measurements, but it is present in measurements with an FTS that uses the same detector to sense the radiance for all spectral channels within a given spectral band. As a result, as shown earlier in Fig. 14, the spectral channel-to-channel noise level is considerably smaller for CrIS than it is for AIRS, leading to the very different vertical resolution of their retrievals. This result is clearly indicated in Fig. 15, which shows that, for AIRS, the difference between the DRDA retrieval errors and the regression (RGN) retrieval errors does not change significantly with a change in vertical layer thicknesses. On the other hand, there is a strong reduction of the DRDA and RGN retrieval error difference with increasing layer thickness for the CrIS. Thus, Fig. 15 shows that the CrIS has higher sensitivity to small-scale vertical profile features than does the AIRS. Moreover, it can be seen that for the DRDA retrievals, there is a large separation (i.e., nearly a factor of 2) between the AIRS and CrIS vertically averaged sublayer mean temperature and humidity errors and that these instrument technology related differences increase as the sublayer thickness decreases, indicating that their retrieval error differences are due, at least on part, to the difference in the vertical resolution between the FTS and GS measurement systems. It can also be seen that the AIRS DRDA retrieval error is not reduced to the CrIS 1-km layer thickness DRDA retrieval error until reaching a 5-km layer thickness. Even for the pure regression retrievals, the sublayer thickness is 2 km greater for AIRS than for CrIS in order to achieve the same sublayer retrieval error level. In summary, both the DRDA and the pure regression retrievals indicate that there is a large vertical resolution difference between the CrIS and AIRS instrument (i.e., FTS versus GS) retrievals. This appears to be a consequence of the factor-of-two difference in their spectral feature measurement fidelity, as shown in Fig. 14.

This difference in vertical resolution of the AIRS GS retrievals and the CrIS FTS retrievals is perhaps most clearly illustrated by looking at a couple of examples of radiosonde comparisons for August 17, 2020 and August 20, 2020. Both the AIRS and CrIS retrievals show the large-scale vertical structure indicated by the radiosonde observations. However, using the RAP forecast profiles as the background profiles for the DRDA retrievals, the CrIS FTS radiances are able to resolve the fine-scale vertical structures of the atmospheric profiles, whereas the AIRS GS radiances do not, as illustrated for the two examples shown in Fig. 16. This result demonstrates the importance of radiance measurement spectral fidelity for being able to optimize the use of Shannon sampling for resolving fine-scale vertical profile features with hyperspectral satellite radiance measurements.

E. Fundamental Advantages of FTS Over a Dispersive (Grating) Sounding Approach

The FTS approach to state-of-the-art hyperspectral sounding has demonstrated a number of practical and fundamental advantages over the grating approach. The fundamental advantages are tied to the FTS capability for realizing the very high spectral fidelity needed to optimize the vertical resolution of temperature

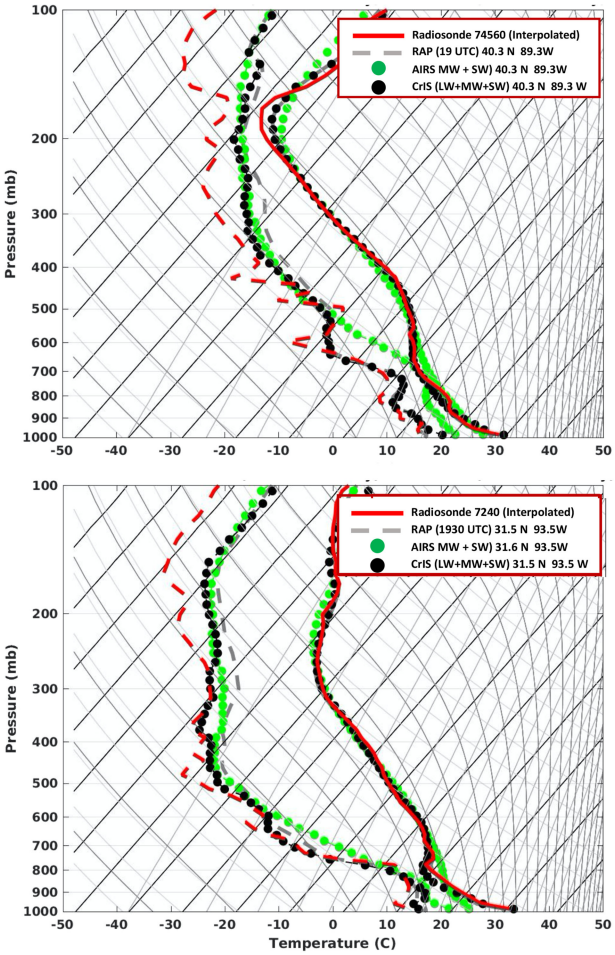

Fig. 16. Comparison between CrIS and AIRS temperature (right) and dew-point temperature (left) retrievals with time and space interpolated nearby radiosonde observations for August 17, 2020 (top panel) and August 20, 2020 (bottom panel). The RAP profile used as the background profile for these DRDA retrievals is shown by the gray lines.

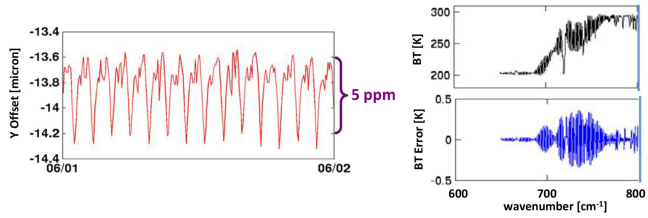

Fig. 17. Orbital variations in spectral calibration for AIRS stemming from very small thermal control variations (±0.02 K per orbit) are shown in the left panel. The ordinate y-offset in microns is a measure of the offset of the optical axis of the AIRS focal plane array with respect to a nominal zero coordinate. The abscissa for the left panel is a 24-h time period (06/01 to 06/02) (credit Larrabee Strow). The repeating pattern demonstrates the 5−6 parts per million (ppm) variation in spectral calibration which occurs every orbit. The corresponding 15-μm CO_2 band brightness temperatures (BT) and BT errors for a 5-ppm spectral shift are shown in the right panel, with errors of 0.6 K peak-to-peak.

and water vapor profiles from passive remote sensing for weather prediction applications.

Here, three fundamental advantages of the FTS approach are summarized to explain why 8 of the 9 hyperspectral IR sounders currently on orbit are based on the FTS approach (AIRS grating from NASA vs. three IASIs from EUMETSAT, two CrISs from NOAA/NASA, the GIIRS and HIRAS from China, and the IKFS-2 from Russia).

1) Spectral Stability: To prevent degradation of the highly accurate radiometric calibration possible with hyperspectral IR sounding instruments (e.g., CrIS is generally better than 0.2 K 3-sigma), it is now known that the spectral calibration should be maintained at about the 1 ppm demonstrated by CrIS [37], [38]. The original specifications of < 10 ppm, later reduced to < 5 ppm, are inadequate.

State-of-the-art FTS instruments can realize this goal by employing dynamically aligned or corner cube interferometers that have excellent immunity to both vibrations and thermal changes. For the FTS, thermal stability is achieved primarily by careful control of the diode laser sampling reference temperature, rather than needing an extremely high degree of control for the whole spectrometer.

The spectral stability goal of 1 ppm is difficult to realize for a grating-based instrument given the fundamental thermal sensitivity of the GS. The AIRS on the EOS Aqua spacecraft is the example of a grating-based hyperspectral sounder that is focused on here since it is the only one to be flown to date. While the whole AIRS spectrometer is thermally stabilized to ±20 mK per orbit, it still has 6 ppm variations in spectral calibration during each orbit. This variation is shown in Fig. 17 (credit Larrabee Strow), along with the radiometric impact of about 0.6 K p-p for 5 ppm variations in the 15-μm CO_2 band. Geographically distributed retrieval artifacts are created by this type of radiance error. In principle, some of this effect could be removed, but no correction has been devised for the real-time use of AIRS data for NWP. It seems likely that any new grating design will need to make a special effort to even match this degree of spectral stability.

2) Intraspectral Artifacts Related to Spatial and Spectral Response Differences: As emphasized by Jim Brault[1] as long ago as the 1970s and 1980s, modern FTS instruments are capable of exceptional spectral fidelity (or degree of exactness). This is a fundamental consequence of the Fourier transform approach that directly provides a well-known instrument line shape (ILS) or spectral response function (SRF), coupled with an accurate spectral calibration made possible by OPD sampling metered by a stable laser. In addition, the fact that the approach naturally provides coverage of broad spectral bands with a single detector avoids subtle spectral artifacts from detector-to-detector property variations. For the grating approach on the other hand, the SRFs are not fundamentally well defined and depend on the detailed geometrical properties of the optical system and the detectors. Since different detectors are used for each spectral channel, subtle calibration errors and correlated noise artifacts can arise which affect the spectral fidelity. Significant detector module-dependent errors can result from both nonuniform scenes when the detectors for different spectral channels within a detector module have slightly different fields of view than

[1]Online. [Available]: https://en.wikipedia.org/wiki/James_W._Brault

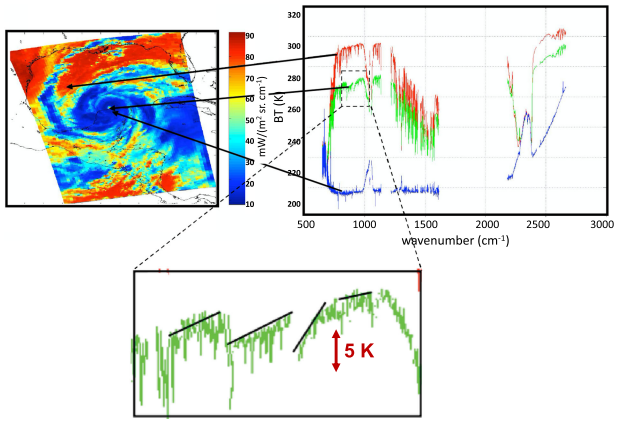

Fig. 18. AIRS spectra from different regions of tropical storm Isadora (September 22, 2002), illustrating the large spectral artifacts that can arise for nonuniform scenes. The red spectrum is from a reasonably clear region of the storm, the blue is from the high clouds surrounding the eye, and the green is from looking mainly in the eye. The very large spectral shape artifacts (up to 5 K) illustrated in the bottom panel result from the variable degree that the different spectral detectors see small amounts of the high clouds surrounding the eye. While this is probably a worst-case example, errors of this kind that are even an order of magnitude smaller would cause significant profiling errors.

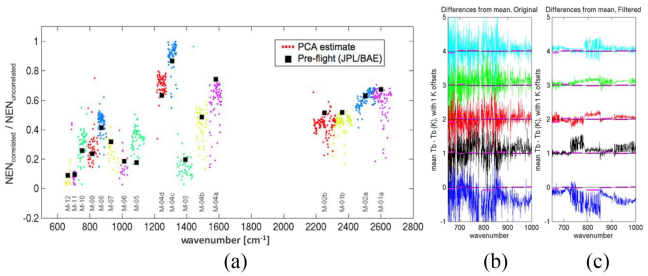

Fig. 19. (a) Ratio of spectrally correlated noise to uncorrelated random noise for AIRS. The correlated noise is at least half as large as the random noise for 9 of the 17 detector arrays used to cover the entire spectrum. (b) Example of AIRS longwave correlated noise spectra isolated from a uniform scene. The five spectra on the left are differences from the mean spectrum over a uniform scene. These spectra are composed of a combination of correlated and uncorrelated noise. (c) Same five differences for spectra that have had the random noise filtered out using a principal component analysis [26], leaving examples of correlated noise. Note that the amplitude of the correlated noise artifacts shown ranges from about 0.2 to 0.9 K, which would be expected to lead to significant temperature profiling errors.

detectors in another module or for uniform scenes from other detector module-dependent calibration effects.

Fig. 18 shows an AIRS example of the very large spectral module-dependent errors that can occur for extremely nonuniform scenes. A far more common situation is that much smaller errors missed by quality control can still create significant profiling errors.

Fig. 19 , from [25], illustrates that there can be significant spectrally correlated artifacts for uniform scenes as well. Panel (a) shows the substantial degree of spectrally correlated noise that routinely occurs for each of the 17 detector arrays of AIRS. Examples of the spectral behavior of this type of correlated noise are shown in panels (b) and (c). These are the types of spectrally correlated errors that cause AIRS temperature retrieval profiles

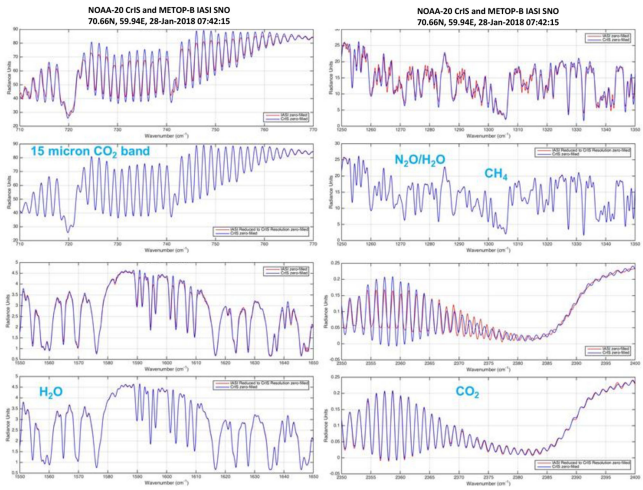

Fig. 20. Two plots in each quadrant of this figure compare a selected region of IASI-B and NOAA-20 CrIS spectra collected during a simultaneous nadir overpass in 2018. The top spectrum in each quadrant shows the native resolution products, and the lower spectrum shows the high degree of agreement when IASI is converted to CrIS spectral properties (difference generally < 0.1 K). Note that at the native resolution, the absorption line amplitudes in this region are actually larger for CrIS than IASI due to the Gaussian apodization routinely applied to IASI spectra. Top left is the LW 15-μm CO_2 band, top right is from the MW water band, lower left is another part of the MW water band, and lower right is from the SW CO_2 band.

to have larger rms errors than those from FTS instruments like IASI and CrIS.

3) Spectral Normalization Among Multiple Instruments: For effective NWP assimilation of a data type, it is necessary to have well-determined sensor properties and error characteristics. To avoid spatially and temporally biased artifacts, this is especially important when multiple sensors are used to give global coverage with rapid temporal sampling. Therefore, it is highly desirable for different instruments of a given type to produce data that can be normalized to common radiometric properties and characteristics.

For hyperspectral IR sounding instruments, several properties are required to be able to transform measured spectra to a common standard for assimilation, namely the following:

1) ILS or SRF;
2) wavelength/wavenumber of spectral samples; and
3) Nyquist sampling of the spectrum to permit rigorous interpolation to a common scale.

For FTS instruments, highly accurate normalization to standard spectral properties is routinely and rigorously performed in a straightforward mathematical process given just a few easily known parameters. For example, routine CrIS processing puts Suomi NPP and NOAA-20 CrIS on a common spectral scale with a common SRF. This is possible because the above-required properties are naturally satisfied by the FTS approach.

On the other hand, for grating instruments, the above properties 1) and 2) are determined by the detailed geometric properties of the grating, detector, and optics that are not straightforward to know or to make exactly alike. For property 1) of AIRS, the SRFs for its 2378 spectral channels had to be measured with an FTS instrument prior to launch. Any new instrument

will need highly accurate characterization of its SRF shapes. For property 2), issues with the spectral scale stability were discussed in Section IV-D. And regarding property 3), not even AIRS is Nyquist sampled everywhere, with its largest shortfalls occurring in the important LW-band. For the grating, achieving the Nyquist sampling necessary for rigorous resampling normalization generally requires large detector arrays (AIRS uses 4756 detectors compared to 27 for CrIS).

After 18 years of AIRS, it can only now be transformed to CrIS-like spectral properties for climate applications in the CHIRP product [39], and some spectral resolution reduction and significant smoothing is still required to reduce comparison errors. Finally, this section is closed with examples of spectral normalization between two quite different FTS instruments, IASI and CrIS. Fig. 20 compares spectra at the native resolution of IASI (max OPD of 2.0 cm with a Gaussian apodization applied) to those of CrIS (max OPD of 0.8 cm, unapodized) and shows how well they can be made to agree by a real-time normalization process. The spectral data are from the mean of one simultaneous nadir overpass chosen for scene uniformity and are spectrally interpolated by zero-filling in the interferogram domain to show the actual absorption line shapes at the measured resolution. CrIS and IASI transformed to CrIS generally agree to brightness temperature differences within ± 0.1 K. This is a testimony to both the excellent spectral and radiometric calibration of each and to the rigor of the normalization procedure.

V. Summary

Shannon sampling theory explains how small-scale vertical profile features can be resolved using high spectral fidelity satellite hyperspectral radiance observations. Rodgers's OE information theory can be used to determine the expected accuracy of atmospheric profiles specified by the assimilation of radiance observations within a numerical prediction model. However, it is shown that for estimating temperature profile accuracy, it is important to exclude water vapor radiance contributions to the temperature profile weighting functions and it is also important to account for the effect of temperature profile specification error when estimating the expected accuracy of water vapor profiles.

The Rodgers IC analysis procedure was applied to CrIS spectral radiances with their associated noise characteristics. It is shown that there is a large loss of vertical temperature and water vapor profile information when only a small subset of CrIS channel radiances, rather than the full CrIS spectrum of radiances, is used for forecast model radiance or retrieval assimilation. The full spectral channel data set is found to provide nearly 1.5 and 2.0 times as much vertical profile IC for temperature and water vapor than does the small carefully selected NCEP sample of 100 CrIS channel radiances that have been assimilated in the GFS model.

The Rodgers information analysis theory shows that the LW measurements play a critical role in providing the sounding IC of the CrIS and AIRS. Large gains of temperature information ($\sim$50%) throughout the troposphere and near surface humidity (as much as factor of $2-3$ within the PBL) are realized by including LW radiance measurements in a numerical model data assimilation of satellite measurements radiances or in profile retrievals.

Analyses of time coincident and geographically overlapping CrIS and AIRS clear sky radiance measurements and retrievals indicate that there is a critical spectral radiance fidelity and profile retrieval vertical resolution advantage of using radiances observed with an FTS instrument rather than radiances observed with a dispersive GS instrument. The AIRS and CrIS radiance and retrieval comparisons analyzed here were restricted to cloud-free atmospheric conditions. For cloudy sky conditions, the difference between spectral radiance noise and associated retrieval accuracy and vertical resolution would be even greater than that shown here due to the enhanced effects of the AIRS detector coregistration errors when viewing nonuniform cloud atmospheric scenes.

The conclusion from both the theoretical radiance measurement IC studies and the empirical CrIS and AIRS radiance and retrieval comparison results is that the atmospheric profile accuracy depends on the spectral resolution, spectral radiance fidelity, and the spectral range (i.e., the number of spectral channels) of the radiance observations used. This result is significant for NWP considering both direct radiance data assimilation as well as for retrieving atmospheric profiles for their assimilation into NWP models. Most important for consideration in the specification of hyperspectral instruments for future polar and geostationary satellites, the FTS approach has very substantial advantages over the dispersive grating approach for realizing the high accuracy needed for tomorrow's advanced sounding instruments. Comparisons between AIRS and CrIS radiance measurements and colocated retrievals illustrate the critical importance of the spectral radiance fidelity found in FTS instruments that favor their use for future hyperspectral sounding radiance measurements. The high vertical resolution atmospheric profile measurements provided uniquely by FTS systems will improve global extended range NWP forecasts as well as improve regional convective weather forecasts, as needed to improve the warning time for life and property threatening localized severe storms. Also, FTS systems enable the rigorous transform of the spectra from multiple instruments to be indistinguishable for NWP data assimilation and climate trend analyses. It is for these reasons that 8 out of the 9 hyperspectral sounders in orbit, on the international system of polar orbiting and geostationary satellites during 2021, are FTS instruments.

Acknowledgment

The authors would like to thank the reviewers of the original manuscript for their comments and criticisms, which led to the improved version for publication. This study was supported by the University of Wisconsin Space Science and Engineering Center under its SSEC2022 program.

References

[1] A. J. Geer *et al.*, "All-sky satellite data assimilation at operational weather forecasting centres," *Quart. J. Roy. Meteor. Soc.*, vol. 144, no. 713, pp. 1191–1217, Nov. 2017.

[2] J. L. Marshall *et al.*, "The joint center for data assimilation," *Bull. Amer. Meteor. Soc.*, vol. 88, no. 3, pp. 329–340, Mar. 2007.

[3] H. Lin, S. S. Weygandt, S. G. Benjamin, and M. Hu, "Satellite radiance data assimilation within the hourly updated rapid refresh," *Wea. Forecasting*, vol. 32, no. 4, pp. 1273–1287, Aug. 2017.
[4] J. R. Eyre, S. J. English, and M. Forsythe, "Assimilation of satellite data in numerical weather prediction. Part I: The early years," *Quart. J. Roy. Meteor. Soc.*, vol. 146, no. 276, pp. 49–68, Feb. 2020.
[5] W. L. Smith, Q. Zhang, M. Shao, and E. Weisz, "Improved severe weather forecasts using LEO and GEO satellite soundings," *J. Atmos. Ocean. Technol.*, vol. 37, no. 7, pp. 1203–1218, Jul. 2020.
[6] W. L. Smith, E. Weisz, S. V. Kireev, D. K. Zhou, Z. Li, and E. E. Borbas, "Dual-regression retrieval algorithm for real-time processing of satellite ultraspectral radiances," *J. Appl. Meteor. Climatol.*, vol. 51, no. 8, pp. 1455–1476, Aug. 2012.
[7] W. L. Smith and E. Weisz, "Dual regression approach for high spatial resolution infrared soundings," in *Comprehensive Remote Sensing*, M. Goldberg, Ed., Oxford, U.K.: Elsevier.
[8] W. L. Smith, Sr., E. Weisz, and H Revercomb, "The retrieval of atmospheric profiles from satellite radiances for NWP data assimilation," in *Proc. Int. TOVS Study Conf.*, 2015. [Online]. Available: http://library.ssec.wisc.edu/research_Resources/publications/pdfs/ITSC20/smith06_ITSC20_2015.pdf
[9] C. D. Rodgers, *Inverse Methods for Atmospheric Sounding - Theory and Practice*. Singapore: World Scientific Press, 2000.
[10] W. L. Smith and H. M. Woolf, "The use of eigenvectors of statistical covariance matrices for interpreting satellite sounding radiometer observations," *J. Atmos. Sci.*, vol. 33, no. 11, pp. 1127–1140, Jul. 1976.
[11] C. D. Rodgers, "Information content and optimisation of high spectral resolution measurements," in *Optical Spectroscopic Techniques and Instrumentation for Atmospheric and Space Research II, SPIE 2380*, P. B. Hays and J. Wang, Eds., 1996, pp. 136–147.
[12] A. D. Collard, "Selection of IASI channels for use in numerical weather prediction," *Quart. J. Roy. Meteor. Soc.*, vol. 133, no. 629, pp. 1977–1991, Dec. 2007.
[13] Y. C. Noh, B. J. Sohn, Y. J. Kim, S. W. Joo, W. Bell, and R. Saunders, "A new infrared atmospheric sounding interferometer channel selection and assessment of its impact on met office NWP forecasts," *Adv. Atmos. Sci.*, vol. 34, pp. 1265–1281, Sep. 2017.
[14] W. P. Menzel, T. J. Schmit, P. Zhang, and J. Li, "Satellite-based atmospheric infrared sounder development and applications," *Bull. Amer. Meteor. Soc.*, vol. 99, no. 33, pp. 583–603, Mar. 2018.
[15] T. J. Schmit, J. Li, S. A. Ackerman, and J. J. Gurka, "High-spectral- and high-temporal-resolution infrared measurements from geostationary orbit," *J. Atmos. Ocean. Technol.*, vol. 26, no. 11, pp. 2273–2292, Nov. 2009.
[16] T. G. Kyle, "Temperature soundings with partially scanned interferograms," *Appl. Opt.*, vol. 16, no. 2, pp. 326–333, 1977.
[17] W. L. Smith, H. B. Howell, and H. M. Woolf, "The use of interferometric radiance measurements for sounding the atmosphere," *J. Atmos. Sci.*, vol. 36, no. 4, pp. 566–575, Apr. 1979.
[18] H. E. Revercomb, H. Buijs, H. B. Howell, D. D. Laporte, W. L. Smith, and L. A. Sromovsky, "Radiometric calibration of IR Fourier transform spectrometers: Solution to a problem with the high-resolution interferometer sounder," *Appl Opt*, vol. 27, no. 15, pp. 3210–3218, 1988.
[19] W. L. Smith *et al.*, "Technical note: Evolution, current capabilities, and future advance in satellite nadir viewing ultra-spectral IR sounding of the lower atmosphere," *Atmos. Chem. Phys.*, vol. 9, no. 15, pp. 5563–5574, Apr. 2009.
[20] C. E. Shannon, "A mathematical theory of communication," *Bell System Tech. J.*, vol. 27, no. 3, pp. 379–423, Jul. 1948.
[21] C. D. Rodgers, "Characterization and error analysis of profiles retrieved from remote sounding measurements," *J. Geophys. Res.*, vol. 95, no. D5, pp. 5587–5595, Apr. 1990.
[22] N. Pougatchev *et al.*, "IASI temperature and water vapor retrievals—Error assessment and validation," *Atmos. Chem. Phys.*, vol. 9, no. 17, pp. 6453–6458, Sep. 2009. [Online]. Available: 10.5194/acp-9-6453-2009
[23] C. D. Rodgers and B. J. Connor, "Intercomparison of remote sounding instruments," *J. Geophys. Res.*, vol. 108, no. D3, Feb. 2003, Art. no. 4116.
[24] R. Eresmaa, J. Letertre-Danczak, C. Lupu, N. Bormann, and A. P. McNally, "The assimilation of cross-track infrared sounder radiances at ECMWF," *Quart. J. Roy. Meteor. Soc.*, vol. 143, no. 709, pp. 3177–3188, Oct. 2017.
[25] D. C. Tobin *et al.*, "Hyperspectral data noise characterization using principal component analysis: Application to the atmospheric infrared sounder," *J. Appl. Remote Sens.*, vol. 1, no. 1, Jun. 2007, doi: 10.1117/1.2757707.
[26] P. Antonelli *et al.*, "A principal component noise filter for high spectral resolution infrared measurements," *J. Geophys. Res.*, vol. 109, no. D23, Dec. 2004, doi: 10.1029/2004JD004862.
[27] J. M. Sieglaff, T. J. Schmit, W. P. Menzel, and S. A. Ackerman, "Inferring convective weather characteristics with geostationary high spectral resolution IR window measurements: A look into the future," *J. Atmos. Ocean. Technol.*, vol. 26, no. 8, pp. 1527–1541, Aug. 2009.
[28] M. T. Chahine *et al.*, "AIRS: Improving weather forecasting and providing new data on greenhouse gases," *Bull. Amer. Meteor. Soc.*, vol. 87, no. 7, pp. 911–926, Jul. 2006.
[29] F. Hilton *et al.*, "Hyperspectral earth observation from IASI: Five years of accomplishments," *Bull. Amer. Meteor. Soc.*, vol. 93, no. 3, pp. 347–370, Mar. 2012.
[30] D. Tobin *et al.*, "Suomi-NPP CrIS radiometric calibration uncertainty," *J. Geophys. Res.*, vol. 118, no. 18, pp. 10589–10600, Sep. 2013.
[31] X. Liu, W. L. Smith, D. K. Zhou, and A. Larar, "Principal component-based radiative transfer model for hyperspectral sensors: Theoretical concept," *Appl. Opt.*, vol. 45, no. 1, pp. 201–209, 2006.
[32] R. Saunders *et al.*, "A comparison of radiative transfer models for simulating atmospheric infrared sounder (AIRS) radiances," *J. Geophys. Res.*, vol. 112, no. D1, Jan. 2007, doi: 10.1029/2006JD007088.
[33] S. Migliorini, "On the equivalence between radiance and retrieval assimilation," *Mon. Wea. Rev.*, vol. 140, no. 1, pp. 258–265, Jan. 2012.
[34] "NOAA combined atmospheric processing system (NUCAPS) – algorithm theoretical basis document." [Online]. Available: https://www.star.nesdis.noaa.gov/jpss/documents/ATBD/ATBD_NUCAPS_v3.0.pdf
[35] "Cooperative institute for meterological satellite studies (CIMSS)/Community satellite processing package (CSPP)." [Online]. Available: http://cimss.ssec.wisc.edu/cspp/
[36] "Hampton university radiosonde/retrieval comparison." [Online]. Available: http://cas.hamptonu.edu/~adinorscia/InteractiveMap/interactivemap.html
[37] Y. Chen, Y. Han, and F. Weng, "Characterization of long-term stability of Suomi NPP cross-track infrared sounder spectral calibration," *IEEE Trans. Geosci. Remote Sens.*, vol. 55, no. 2, pp. 1147–1159, Nov. 2017.
[38] L. L. Strow *et al.*, "Spectral calibration and validation of the cross-track infrared sounder on the Suomi NPP satellite," *J. Geophys. Res. Atmos.*, vol. 118, no. 22, pp. 12486–12496, Nov. 2013.
[39] L. L. Strow, S. DeSouza-Machado, S. Leroy, H. Motteler, C. Hepplewhite, and S. Buczkowski, "Climate hyperspectral infrared product (CHIRP): Radiometric stability and trends," in *Proc. Fall 2018 NASA AIRS Sci. Team Meeting*, Greenbelt, MD, USA, 2018.

William (Bill) Smith received the Ph.D. degree in meteorology from the University of Wisconsin–Madison in 1966.

He is an Active Remote Sensing experimentalist. He was a Principal Investigator of successful research satellite sounding and Earth radiation budget experiments and pioneered the hyperspectral resolution sounding technique being used for the current and future international polar and geostationary satellite infrared atmospheric sounding systems. He has led atmospheric research groups at National Oceanic and Atmospheric Administration (NOAA), Washington, DC, USA; National Aeronautics and Space Administration (NASA), Washington, DC, USA; University of Wisconsin, Madison, WI, USA; and Hampton University, Hampton, VI, USA.

Prof. Smith developed the first satellite atmospheric sounding retrieval algorithm used for operational meteorology for which he received the Department of Commerce Gold Medal Award. He has also served as the President of the International Radiation Commission.

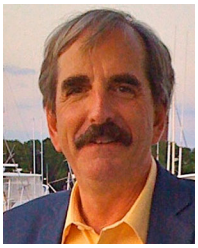

Henry (Hank) E. Revercomb received the B.S. degree in physics from Union College, Schenectady, NY, USA, in 1966, the M.S. and Ph.D. degrees in theoretical physics from the University of Wisconsin-Madison, Madison, WI, USA, in 1969 and 1972, respectively.

Since 1974, has worked with the Space Science and Engineering Center (SSEC), University of Wisconsin-Madison, serving as its Director from 1999–2016. He continues to use radiation measurements to study the atmospherics of Earth and other planets. His specialties include high spectral resolution instrumentation for atmospheric remote sensing and spectroscopy, operational temperature and water vapor sounders, climate observing systems, and net radiative flux observations of Venus and Jupiter.

Elisabeth Weisz received the M.S. degree in theoretical physics and the Ph.D. degree in geophysics and meteorology , in 1998 and 2001, respectively, from the University of Graz, Graz, Austria.

She has been with the Space Science and Engineering Center (SSEC), University of Wisconsin-Madison, Madison, WI, USA, since 2001. She is currently serving as a Senior Scientist. Her research focuses on the development, evaluation, and application of atmospheric sounding retrieval algorithms using satellite-based high-spectral resolution infrared radiance measurements. Her work also includes multisatellite/instrument data fusion, radiative transfer modeling, and software development for polar-orbiting direct broadcast data processing.

David C. Tobin received the B.S., M.S., and Ph.D. degrees in physics from the University of Maryland Baltimore County, Baltimore, MD, USA, in 1991, 1993, and 1996, respectively.

He is a Distinguished Scientist with the Cooperative Institute for Meteorological Satellite Studies (CIMSS) within the Space Science and Engineering Center (SSEC), University of Wisconsin-Madison, Madison, WI, USA. His research interests include infrared molecular spectroscopy, infrared radiative transfer, hyperspectral sensor design, calibration, and data processing, and satellite intercalibration.

Dr. Tobin is a member of the International Radiation Commission, the Global Space-Based Inter-Calibration System (GSICS) Research Working Group and the International TOVS Advanced Sounder Working Group.

Robert O. Knuteson received the Ph.D. degree in physics from the University of Wisconsin-Madison (UW-Madison), Madison, WI, USA, in 1987.

He has been with the Space Science and Engineering Center, UW-Madison since 1987. His research interests include infrared satellite sensor calibration and atmospheric remote sensing.

Joe K. Taylor was born in Regina, Saskatchewan, Canada. He received the B.Eng. and M.S. degrees in engineering physics from the University of Saskatchewan, Saskatoon, SK, Canada, in 1994 and 2000, respectively, and the Ph.D. degree in electrical engineering from University of Laval, Quebec, QC, Canada, in 2014.

He was a Research Assistant with the University of Saskatchewan Institute of Space and Atmospheric Studies from 1999 to 2003. Since 2003, he has been a Researcher with the University of Wisconsin-Madison Space Science and Engineering Center (SSEC), Madison, WI, USA. His research interests include hyperspectral infrared instrumentation, infrared spectroradiometer calibration and validation, and optical system design and analysis.

W. Paul Menzel received the Ph.D. degree in physics from the University of Wisconsin-Madison (UW), Madison, WI, USA, in 1974.

He explored possibilities for sounding the Earth's atmosphere from satellites at the UW Space Science and Engineering Center (SSEC), Madison, WI, USA. In 1983, he joined National Oceanic and Atmospheric Administration (NOAA), Washington, DC, USA, to develop and test new remote sensing environmental products. Since 2007, as a Senior Scientist with SSEC, he has been studying cloud and water vapor trends as well as synergy of high spatial resolution imaging with high spectral resolution sounding instruments.

Dr. Menzel is a Fellow of the American Meteorological Society and recipient of the Yuri Gagarin Medal for his decades of contributions to environmental satellite applications research and training.